Int J Thermophys (2009) 30:619–634
DOI 10.1007/s10765-009-0558-6

A Study on the Effect of Thermal Ageing on the Specific-Heat Characteristics of 9Cr–1Mo–0.1C (mass%) Steel

B. Jeyaganesh · S. Raju · S. Murugesan · E. Mohandas · M. Vijayalakshmi

Received: 4 October 2007 / Accepted: 6 January 2009 / Published online: 3 February 2009

Abstract The effect of thermal ageing on the heat-capacity behavior of 9Cr–1Mo–0.1C (mass%) ferritic/martensitic steel has been studied using differential scanning calorimetry (DSC) in the temperature range from 473 K to 1,273 K. The DSC results in the case of slow cooled, normalized and tempered, and subsequently thermally aged samples (500 h to 5,000 h at 823 K (550 °C) and 923 K (650 °C), clearly marked the presence of both magnetic and α-ferrite + carbide $\rightarrow$ γ-austenite phase transformations that take place successively upon heating. Furthermore, for the case of fully martensitic microstructure, an additional exothermic transformation at about 920 K (647 °C), arising from carbide precipitation is noticed. This event is characterized by a sharp drop in C_P. It is found that the α-ferrite + carbide $\rightarrow$ γ-austenite phase transformation temperature is only mildly sensitive to microstructural details, but the enthalpy change associated with this phase transformation, and especially the change in specific heat around the transformation regime, are found to be dependent on the starting microstructure generated by thermal ageing treatment. Prolonged ageing for about 500 h to 5,000 h in the temperature range from 823 K to 923 K (550 °C to 650 °C) contributed to a decrease in heat capacity, as compared to the normalized and tempered sample. This is due to the increase in carbide volume fraction. The martensitic microstructure is found to possess the lowest room-temperature C_P among different microstructures.

Keywords Ferritic steel · Heat treatment · Martensite · Specific heat · Tempering

B. Jeyaganesh · S. Raju (✉) · S. Murugesan · E. Mohandas · M. Vijayalakshmi
Physical Metallurgy Division, Materials Development and Characterisation Group, Indira Gandhi Centre for Atomic Research, Kalpakkam, 603 102, Tamil Nadu, India
e-mail: sraju@igcar.gov.in

1 Introduction

A study on Cr–Mo based ferritic–martensitic steels is of interest and relevance on both basic and applied grounds. It is well known that ferritic steels have seen extensive applications in conventional as well as nuclear power plants [1–3]. With the emerging impetus to improve the power generation efficiency in thermal power plants and also due to the changing priorities in the area of nuclear fuel options in promoting advanced liquid metal-cooled fast reactor concepts, there is a resurgent interest in the development of advanced high-temperature ferritic steels with enhanced creep resistance [4–6]. Added to this is the fact that certain special ferritic steels like the reduced activation ferritic–martensitic (RAFM) steels containing tungsten and tantalum in place of molybdenum and niobium are also under consideration for application in fusion reactors [7]. On the basic front, the phase and microstructural changes that take place in a ferritic steel during the course of long exposure to high-temperature service conditions, constitute an interesting playground for understanding many a basic issue related to alloy phase equilibria, diffusional phase transformations, and transformation kinetics.

Although the physical metallurgy of standard Cr–Mo steels is replete with many experimental and theoretical investigations on phase stability and microstructure evolution during heat treatments [8–21], there seems to be a general paucity of experimental data on various thermodynamic quantities [20]. It is clear that a consistent thermodynamic data set is essential from the point of view of understanding as well as predicting the long-term phase stability of alloys [10,16–18]. The microstructure of ferritic steels being very sensitive to heat treatment [15,19], it is probable that the thermodynamic quantities measured thereof may exhibit certain microstructural dependence, in direct relation to the phase fractions of different microstructural constituents present in the alloy. A preliminary survey of literature on this account has revealed that the effect of different starting microstructures on the heat capacity of high chromium steels, especially the enthalpy changes associated with phase transformations has not been investigated to date. In view of this fact, this study is oriented toward characterizing the effect of typical ageing treatments on the heat capacity of a nuclear grade 9Cr–1Mo steel. The heat capacity is measured using high-temperature differential scanning calorimetry (DSC) in the temperature interval from 473 K (200 °C) to 1,273 K (1,000 °C). The experimental details are given below.

2 Experimental Details

2.1 Ageing Treatments and General Characterization of Microstructure

The chemical composition (mass%) of the steel used in this study is as follows: 8.44Cr, 0.94Mo, 0.49Si, 0.46Mn, 0.17Ni, 0.11Cu, 0.1C, 0.008P, 0.011Al, 0.002S, 0.001V, 0.008N, and balance being Fe. The alloy has been supplied in plate form in normalized and tempered (N&T) condition, which corresponds to austenitization at 1,323 K (1,050 °C) for 15 min, followed by air cooling to room temperature. Subsequent tempering is carried out at 1,053 K (780 °C) for 2 h, and the tempered sample is air cooled

to room temperature. In this study, a set of samples is further subjected to the following thermal ageing schedules:

(i) ageing at 823 K (550 °C) for 500 h,
(ii) ageing at 823 K (550 °C) for 5,000 h, and
(iii) ageing at 923 K (650 °C) for 500 h.

In order to study the thermal effects that accompany the tempering reaction of a fully martensitic microstructure, a few samples are directly quenched at 1,323 K (1,050 °C) to obtain fully martensitic microstructure. For basic metallography, X-ray diffraction and micro-hardness measurements, the samples were prepared in the standard manner.

The optical micrographs of different samples are presented in Fig. 1 . The martensitic character of the quenched sample is immediately apparent from Fig. 1a. The presence of numerous laths emanating from prior austenite boundaries is readily seen from Fig. 1a. In Fig. 1b–d, which characterizes the N&T and aged samples, the presence of profuse, tiny carbide particles decorating the prior austenite grain boundaries, and ferrite sub-grain boundaries is clearly seen. It may be noted that compared to an 823 K (550 °C)/500 h aged sample (Fig. 1c), the 923 K (650 °C)/500 h ageing

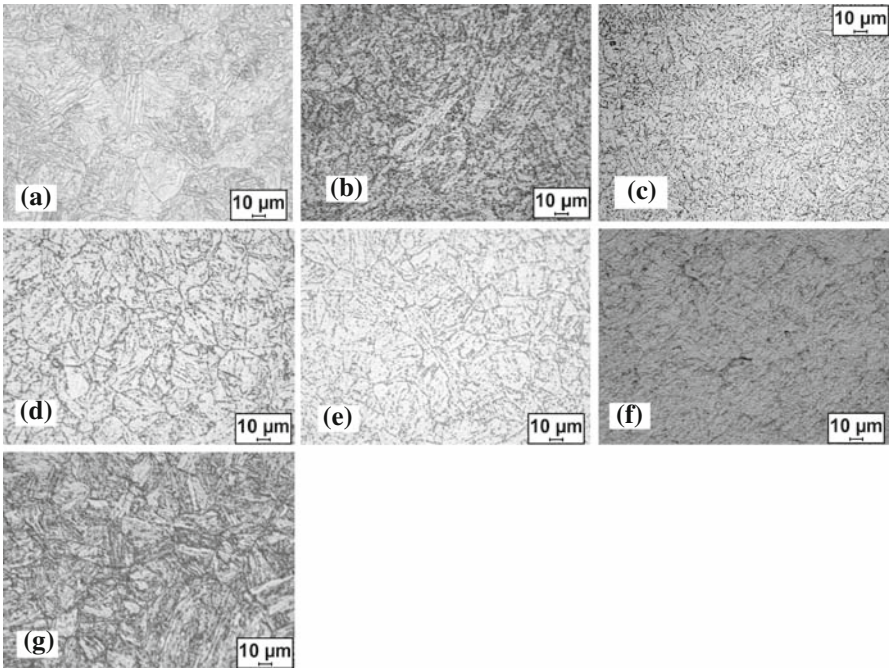

Fig. 1 Optical microstructures of 9Cr–1Mo steel in different heat-treated conditions: (**a**) quenched from 1,323 K (1,050 °C); martensitic microstructure, (**b**) normalized and tempered (N&T) microstructure, (**c**) N&T + ageing at 823 K (550 °C) for 500 h, (**d**) N&T + ageing at 823 K (550 °C) for 5,000 h, (**e**) N&T + ageing at 923 K (650 °C) for 500 h, (**f**) carbide precipitation in martensite: quenched from 898 K, and (**g**) carbide precipitation in martensite: quenched from 973 K

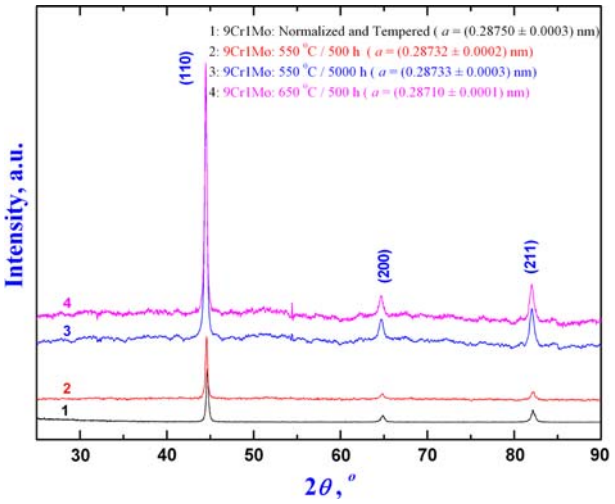

Fig. 2 Room temperature X-ray diffraction profiles of 9Cr–1Mo steel

treatment results in a slightly coarsened ferrite grain structure (Fig. 1e), however, with no appreciable change in carbide particle density or its general morphology. On the other hand, it is clearly seen that compared to N&T microstructure (Fig. 1b), the longer durations (500 h to 5,000 h) of ageing at 823 K (550 °C) produces a better definition of the ferrite grain structure (compare Fig. 1c, d). For the case of plain 9Cr–1Mo 0.1C steels, it has already been established that prolonged thermal ageing in the temperature range from 823 K to 923 *K* (550 °C to 650 °C) results in the precipitation of $(Cr, Fe)_{23}C_6$ type carbide, the composition, size, and distribution of which are sensitive to ageing time and temperature [9]. A higher ageing temperature and longer time durations are conducive to realizing equilibrium and hence a higher volume fraction of the carbide phase. On the contrary, ageing to very long durations such as 1,000 h may mark the onset of carbide particle coarsening and a resulting change in their morphology. It emerges therefore that the starting microstructure in the case of aged samples is one of containing a relaxed ferrite matrix in which the carbide particles are dispersed along grain and sub-grain boundaries, in addition to a few in the grain interior.

The room-temperature X-ray diffraction profile, taken with the INEL® diffraction system using Cu-Kα radiation, of various samples are collated in Fig. 2. Because of the strong fluorescence background, the relatively weak reflections of the carbide phase are not readily visible in the pattern. The average value of the lattice parameter of the ferrite phase, after due correction by the Nelson–Riley procedure, is found to be (0.287 ± 0.003) nm (Table 1). It may be mentioned that within the limits of experimental uncertainty, the lattice parameter of the ferrite phase did not exhibit any noticeable dependence on the microstructural character. The hardness values of different microstructures are measured using a Leitz micro-hardness tester, employing a load of 50 g. The measured hardness and lattice parameter values for various samples are listed in Table 1.

Table 1 Transformation temperatures due to magnetic (T_C) and α-ferrite + carbide $\rightarrow$ γ-austenite phase change (Ac_1, Ac_p, Ac_3) together with the enthalpy change associated with the α-ferrite + carbide $\rightarrow$ γ-austenite, transformation as obtained in this study are tabulated. Also, the α-*ferrite* lattice parameter and the micro-hardness values of different heat-treated 9Cr–1Mo steel samples are listed. The negative sign for $\Delta^\circ H$ for carbide precipitation from martensite is suggestive of the exothermic nature of precipitation

Sample designation	T_C (K)	Ac_1 (K)	Ac_p $\alpha \rightarrow \gamma$ peak temperature (K)	Ac_3 (K)	$Ac_3 - Ac_1$ (K)	Peak area for $\alpha \rightarrow \gamma$ transformation ($\mu V \cdot s \cdot mg^{-1}$)	$\Delta^\circ H^{\alpha \rightarrow \gamma}$ ($J \cdot g^{-1}$)	Hardness under 100 g load (VHN)	Ferrite lattice parameter (nm)
Pure iron	1,040	1,156	1,184	1,200	44	2.58	16	169	
9Cr–1Mo: N&T	1,013	1,094	1,115	1,143	49	2.25	15	274	0.2875 ± 0.0003
9Cr–1Mo: 823 K (550 °C)/500 h	1,014	1,095	1,115	1,146	51	2.07	12	254	0.2873 ± 0.0002
9Cr–1Mo: 823 K (550 °C)/5,000 h	1,015	1,099	1,116	1,150	51	2.31	13	274	0.2873 ± 0.0003
9Cr–1Mo: 923 K (650 °C)/500 h	1,015	1,100	1,117	1,148	48	2.10	13	287	0.2871 ± 0.0001
9Cr–1Mo: Martensite	1,011	1,092	1,112	1,145	53	2.25	15	464	–
Carbide precipitation peak data in martensite		$T_{ps} = 881$	$T_{peak} = 920$	$T_{pf} = 947$	$T_{ps} - T_{pf} = 66$	0.8533	−5.6	331	–

2.2 C_P Measurements Using DSC

The samples for DSC experiments were sliced from the heat-treated plate using a diamond-coated wire saw. These were further cleaned and polished to regular and nearly identical shapes of mass with a range of (50 to 100 ± 0.1) mg. The DSC experiments were performed with a Setaram Setsys 16® heat-flux type high-temperature differential scanning calorimeter, employing recrystallized alumina crucibles of about 100 µL volume. The description of the equipment and the calibration procedure has been discussed in a previous publication [22]. Stated briefly, the experiments were performed under a constant flow ($50\,\mathrm{mL \cdot min^{-1}}$) of high purity (99.999 %) argon. A heating rate of $10\,\mathrm{K \cdot min^{-1}}$ is employed. While lower heating rates resulted in mild decarburization of the sample due to appreciable resident time at high temperatures, very high heating rates are not normally recommended for specific-heat studies, especially due to the large thermal lag between the actual sample temperature and that sensed by the noncontact probe. By calibrating the sample heat flow against the pure iron reference signal, especially around the region of phase transformations, the temperature lag in the case of ferritic steel for a heating rate of $10\,\mathrm{K \cdot min^{-1}}$, is estimated to be $\leq 2\,\mathrm{K}$. The sample mass and shape have been kept nearly the same for both the reference as well as steel sample in this case. Fresh samples were used for each run, and multiple runs under identical conditions are performed for calibrating the precision of the measured transformation temperature. The temperature calibration is performed using recommended high pure melting point standards, namely, Sn, Al, Pb, In, and Au. In addition, the measurement of the enthalpy of the $\alpha(\mathrm{bcc}) \rightarrow \gamma(\mathrm{fcc})$ allotropic transformation in pure iron (Aldrich, impurities $\leq 80\,\mathrm{ppm}$) under identical experimental conditions is also employed for the heat flow calibration. The heat-flow rate or specific-heat calibration is performed using literature data for the specific heat of pure iron [23,24]. The measured transformation temperatures are accurate to $\pm 2\,\mathrm{K}$; the transformation enthalpies are accurate to ± 5 % at $10\,\mathrm{K \cdot min^{-1}}$. Since in ferritic steels, the microstructure resulting upon cooling from the austenite phase is sensitive to the cooling rate, it is not advisable to use the cooling part of the DSC profile in an analysis that focuses on studying the effect of various initial microstructures on the temperature variation of heat capacity. Moreover, a reliable and reproducible temperature and heat-flow calibration of a DSC for a cooling cycle mean a comparatively difficult proposition. Accordingly, the enthalpy and the heat-flow calibration of the signal were carried out only for the heating cycle in this study.

A typical heat-capacity measurement using DSC in the continuous heating mode involves recording of at least three consecutive, non-stop experimental runs under identical heating, holding, and cooling schedules [25,26]. In this study, the experimental schedule consisted of heating the system from room temperature to an initial temperature of 473 K (200 °C) at a rate of $10\,\mathrm{K \cdot min^{-1}}$ and holding at this temperature for about 15 min. This is required for the attainment of thermal equilibrium of the system before starting any measurement. This is followed by the actual programmed heating, holding, and cooling schedules. In this study, the sample is heated at a steady rate of $10\,\mathrm{K \cdot min^{-1}}$ to 1,273 K (1,000 °C), followed by an isothermal hold of about 15 min at this temperature. Subsequently, the sample is cooled to 473 K at $10\,\mathrm{K \cdot min^{-1}}$ and is allowed a resident time of 15 min at this temperature, before it is finally cooled again

to room temperature. The three basic DSC runs that constitute a C_P measurement are [25,26]:

(i) the baseline run employing only identical empty crucibles on both sides of the DSC plate,
(ii) the reference or calibration run with the sample crucible containing pure iron of known mass, and
(iii) the sample run with a known mass of ferritic steel loaded onto the sample crucible.

It must be noted that all the three runs were performed under identical experimental conditions. In this study, we augmented this scheme by performing one more additional baseline run at the end of the abovementioned three-run schedule. This was done in order to ensure or assess the extent of the baseline reproducibility at the end of each experimental schedule. A good agreement between the start and finish baselines is suggestive of the stable thermal dynamics of the entire DSC module and the temperature sensor. Moreover, it also implies that the sample side crucible remains fairly uncontaminated during the course of the experiment.

The following formula, based on the method of ratios has been used to calculate C_P, from the three-run DSC data [26]:

$$C_P^{\mathrm{S}} = C_P^{\mathrm{R}} \times (m_{\mathrm{R}}/m_{\mathrm{S}}) \times \{(\mu_{\mathrm{S}} - \mu_{\mathrm{b}}) / (\mu_{\mathrm{R}} - \mu_{\mathrm{b}})\}. \quad (1)$$

In the above expression, C_P^{S} and C_P^{R} represent the specific heat of the sample and the reference whose masses are given by m_{S} and m_{R}, respectively. μ_{S} is the microvolt DSC signal obtained with the sample, μ_{R} is the corresponding signal obtained with the reference or standard material, and μ_{b} is the baseline signal obtained with empty crucibles.

3 Results

3.1 Principal Transformation Characteristics

In Fig. 3, a set of typical DSC profiles obtained during the heating cycle with the steel sample, pure iron, and with empty crucibles (baseline) is presented. In order to illustrate the role of starting microstructure on the nature of the DSC thermogram, the profile of the normalized and tempered (N&T) sample is compared with that of the nearly 100 % martensite microstructure. It is clear from Fig. 3, that in the temperature range of interest, two well-resolved endothermic peaks characterize the DSC profiles of pure iron and N&T steel samples. The first peak marked as T_{C}, arises from the ferromagnetic-to-paramagnetic transformation, while the second one is due to the α-ferrite + carbides $\rightarrow$ γ-austenite phase change that occurs on crossing the Ac_1 temperature. In the literature, it is conventional to represent the onset temperature of the α-ferrite + carbide $\rightarrow$ γ-austenite transformation as Ac_1 and the offset point as Ac_3. It is also noteworthy that in the case of a steel sample, the Curie point and the onset (Ac_1), peak (Ac_p), and finish (Ac_3) temperatures for the $\alpha \rightarrow \gamma$ structural transformations are lower than those of the corresponding values for pure iron. For

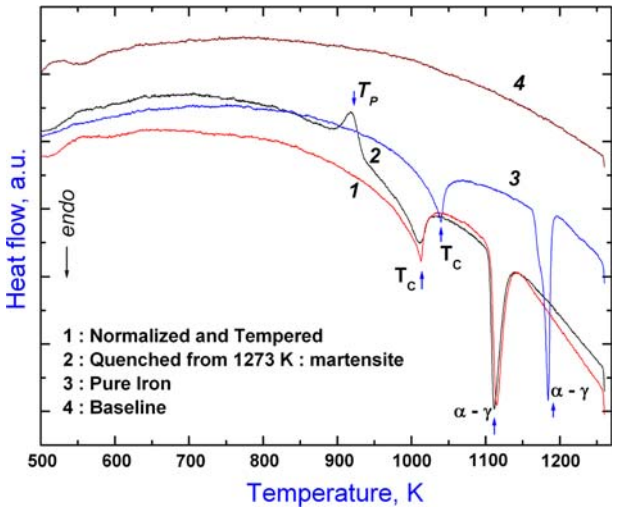

Fig. 3 Typical DSC profiles of 9Cr–1Mo steel in N&T and martensitic conditions. Profile of iron is given for reference

the case of martensite, an extra exothermic peak is observed at about 920 K (647 °C) (see Fig. 3). This peak, corresponding to the precipitation of $M_{23}C_6$ type carbide from virgin martensite [27], is, however, absent in the DSC profiles of tempered and aged samples. This is because of the fact that the carbide precipitation had already been realized to almost full measure in these samples during prior tempering and subsequent long-ageing treatments [9]. The enthalpy change ($\Delta^\circ H$) associated with the magnetic transition, $\alpha \rightarrow \gamma$ structural change, and $M_{23}C_6$ carbide precipitation reactions are directly obtained from the DSC profile as the total or integrated area of the respective peaks. The determination of the calibration factor ($J \cdot \mu V^{-1} \cdot s^{-1}$) for converting the peak area into appropriate enthalpy units is enabled from a knowledge of the known value of the enthalpy associated with similar phase changes taking place in pure iron and the corresponding peak area—all measured under identical experimental conditions. It is reasonable to assume in the case of pure iron that for a heating rate of about $10\,K \cdot min^{-1}$, the $\alpha \rightarrow \gamma$ allotropic transformation goes to near completion; but in the case of high chromium steels, the presence of carbides and its sluggish dissolution in austenite, results in an incomplete realization of the $\alpha \rightarrow \gamma$ transformation at the transformation off-set Ac_3 temperature [21,28,29]. Because of this fact, there is a mild underestimation of the true enthalpy change that is associated with austenite formation reaction under equilibrium conditions. In Table 1, the $\alpha \rightarrow \gamma$ transformation onset (Ac_1) and offset (Ac_3) temperatures, and the associated transformation enthalpy ($\Delta^\circ H_{tr}$) values measured in this study are listed.

In general, the Curie (T_C) temperature turns out to be relatively insensitive to the effects of ageing (Table 1). However, Ac_1 and Ac_3 values show slight microstructure sensitivity. In general terms, ageing serves to increase the austenite start (Ac_1) temperature. It is also instructive to note that in the case of martensite, the width of the $\alpha \rightarrow \gamma$transformation zone as measured by the difference in the offset and onset

points, that is $Ac_3 - Ac_1$, is the highest recorded in this study. This suggests that for a given heating rate, the presence of considerable strain in the starting martensitic microstructure serves to retard the overall kinetics of reaustenitization reaction upon heating. Considering the scope of this study, the energetics and kinetic aspects of tempering are not studied here.

The measured enthalpy change $\Delta^\circ H_{\mathrm{tr}}$ associated with α-ferrite + $M_{23}C_6$ $\rightarrow$ γ-austenite transformation in 9Cr–1Mo steel is slightly smaller than the corresponding $\alpha \rightarrow \gamma$ value for pure iron [23,24] (see Table 1); but as mentioned before, the austenite formation seldom goes to 100 % completion at the Ac_3 temperature; often it takes a little superheating depending on composition and heating rate to get the so-called homogeneous austenite [30].

3.2 Ageing Induced Changes in C_P

In Fig. 4a–f, the measured C_P data for the aged samples of 9Cr–1Mo steel are grouped together. Although, the qualitative nature of the C_P curve remains much the same for all the samples other than the one that had martensite as the starting microstructure, the specific points described below deserve special mention. Not withstanding the maximum uncertainty of about ±5 % (this pertains to the temperature range from 850 K to 1,200 K; for lower temperatures, the average C_P data are accurate to about ±(2 to 3) %) associated with the present heat-capacity data; the room temperature C_P of the normalized and tempered (N&T) sample (Fig. 4a) is distinctly higher than that of the aged ones. In other words, ageing brings down the C_P values. This is due to the fact that long-time ageing serves to increase the volume fraction of the carbide phase. Furthermore, among the aged samples, the 923 K (650 °C)/500 h aged sample has higher heat capacity than the 823 K (550 °C)-aged one. An appeal to their respective microstructures (Fig. 1) suggests that the 923 K (650 °C)-ageing treatment has resulted in a refinement or coarsening of the ferrite grain size, besides a marginal increase in carbide density. As mentioned before, the choice of a higher ageing temperature, namely, 923 K (650 °C), results in the development of a more relaxed martensite and hence a higher C_P. In a similar vein, it can also be noticed that an increase of ageing time from 500 h to 5,000 h at 823 K (550 °C) has served to decrease C_P by a small amount (compare the C_P curves (b) and (c) in Fig. 4f). Thus, it may be inferred in general terms that prolonged ageing, accompanied by a concomitant increase in carbide volume fraction and a change in its composition induces a decrease in C_P.

An attempt to quantify the carbide particle number density and its apparent morphological attributes from the secondary electron images by means of Image J software revealed that compared to 500 h aged samples, 5,000 h ageing at 550 °C induced an increase in particle density by 8 %. The apparent particle size (measured as half of the major axis assuming an ellipsoidal shape) also showed an increase from 0.05 µm to 0.2 µm. An increase in the ageing temperature to 650 °C on the other hand, resulted in an enhancement of the ferrite sub-grain size rather than the carbide particle density. It should be noted that quantification of ferrite sub-grain sizes in a rigorous sense is fraught with difficulty since a precise assignment of an image attribute was not possible in this case. Although this study's results have no absolute meaning and are subject

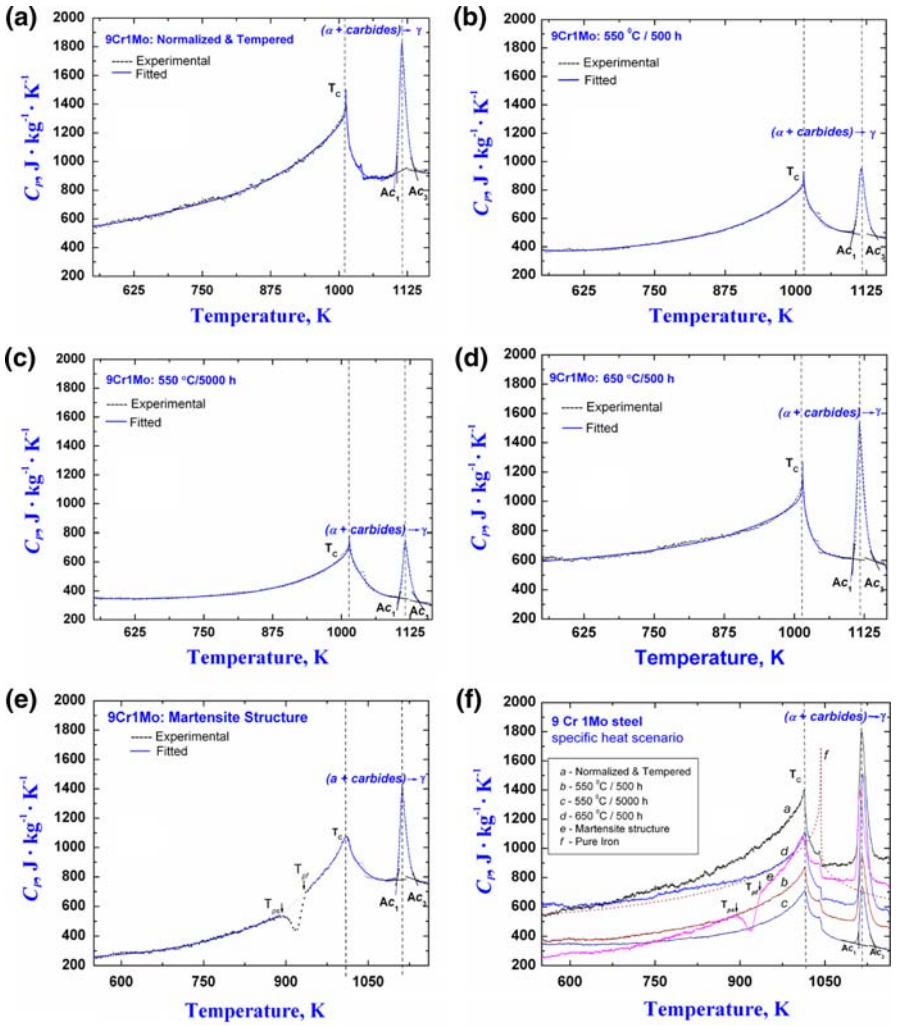

Fig. 4 Temperature variation of C_P of 9Cr–1Mo steel in different heat-treated conditions: (**a**) N&T, (**b**) 823 K/500 h aged, (**c**) 823 K/5,000 h, (**d**) 923 K/500, (**e**) martensite, and (**f**) overall scenario. C_P of pure iron is also presented for comparison (dotted line). The error bar indicated is typical of the study measurements

to certain errors arising from setting the threshold values for certain image attributes, we believe that a certain degree of sub-grain growth and refinement was noticed in 650 °C-aged samples and this is believed to be responsible for the observed change in C_P.

The heat capacity of martensite on the other hand, starts with a lower value, but quickly rises upon approaching T_{ps}, the $M_{23}C_6$ precipitation start temperature (see Fig. 4f). At T_{ps}, the carbide precipitation causes a drop in the specific heat, and on reaching T_{pf}, the apparent precipitation finish temperature, C_P increases once again to

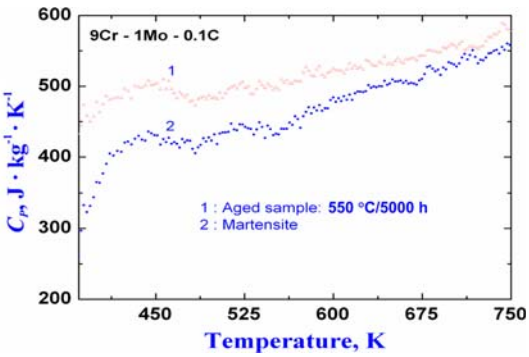

Fig. 5 Comparison of the temperature variation of C_P of martensite with that of the aged sample in the intermediate temperature range

catch up with the 923 K (650 °C -aged sample). In order to assess the nature of microstructure that existed just around the carbide precipitation temperature, a martensite sample was heated at the rate of $10\,\mathrm{K}\cdot\mathrm{min}^{-1}$ to 898 K (625 °C in DSC, kept at this temperature for 1 s, and then fast-cooled to room temperature at $99\,\mathrm{K}\cdot\mathrm{min}^{-1}$. It must be mentioned that the carbide precipitation start temperature (T_{ps}) is about 881 K, and therefore it is clear that at 898 K, the carbide precipitation would have just begun. It is presumed that the fairly high cooling rate employed is adequate to preserve the nascent microstructure that existed at 898 K. In a similar fashion, another martensite sample was heated to 973 K, a temperature slightly ahead of the carbide precipitation finish temperature ($T_{\mathrm{pf}} = 947\ K$), and is rapidly cooled at $99\,\mathrm{K}\cdot\mathrm{min}^{-1}$ to room temperature. The optical micrographs of these two quenched-in samples are illustrated in Fig. 1f, g, respectively. The difference between these two microstructures is indeed striking. While the sample quenched from 898 K is somewhat featureless and revealed barely any sign of precipitation, the sample quenched from 973 K contained copious amount of carbides. However, the ferrite matrix grain structure has not been very well refined yet.

As for as martensite samples are concerned, we have also performed one additional C_P measurement in the 100 °C to 500 °C temperature interval, especially to see, if any appreciable heat effects are involved in the process of martensite relaxation just prior to the onset of tempering. The results of this study are illustrated in Fig. 5. As may be seen, the C_P of virgin martensite is lower than that of the aged sample, but this difference is quickly diminishing with increasing temperature. This observation implies that, upon the onset of thermally assisted relaxation of martensitic microstructure involving the relief of lattice strain and rearrangement of dislocation substructure, the heat capacity variation of martensite becomes very similar to that of the aged sample.

3.3 Analytical Representation of C_P Versus Temperature Data

Since, as is evident from Fig. 4, the temperature variation of C_P is highly complex in the investigated range of temperature, namely, 473 K to 1,273 K, it is not possible to fit analytically the entire C_P (T) data in terms of a single, simple expression. In view of this, it was decided to obtain piece-wise numerical representation in three discrete temperature intervals using the following functional form suggested by Kempen et al. [31]:

$$C_P(T) = A + BT + CT^2 + DT^{-2} + E\exp\left(FT^*\right)\left(T^*\right)^G. \quad (2)$$

where

$$T^* = (T - T_R)/T_R, \quad (3)$$

and $T_R = T_C$ in the first temperature interval $473\,K \leq T \leq T_C$ covering the ferromagnetic α-ferrite + carbide two-phase regime. For temperatures higher than T_C but less than Ac_1, that is, $T_C \leq T \leq Ac_1$, another fit is attempted, with the definition of T^* maintained as given in Eq. 3. In the third temperature interval corresponding to $Ac_1 \leq T \leq Ac_3$, a third fit has been effected, keeping the definition of T^* as given by

$$T^* = (T - Ac_p)/Ac_p. \quad (4)$$

For martensite, a four-zone fit is attempted due to the additional carbide precipitation occurring at 923 K (650 °C). In Table 2, the values for different coefficients figuring in Eq. 2 for each sample are presented. The values of T_C and Ac_p used in the fitting procedure are listed in Table 1. In Fig. 4a–f, the fitted C_P values are compared with the measured ones. It is clear from this figure that Eq. 2 fits the data rather well. However, it must be added that in the transformation temperature domain, the goodness of the fit is very sensitive to the values of coefficients and it is for this reason that these values are listed to four significant digits in Table 2.

4 Discussion

Although there have been many instances of application of thermal analysis methods for the study of tempering kinetics and phase transformation energetics in steels and in other iron-based alloys [32–39], there are not many studies devoted to incorporating the effect of microstructural changes on the thermodynamic properties of ferritic steels. Krielaart et al. [33], for example, have used DSC to study the enthalpy effects associated with the $\gamma \rightarrow$ pearlite, and $\gamma \rightarrow \alpha$-ferrite + pearlite transformations during cooling of low-carbon eutectoid and hypo-eutectoid steels from single-phase austenite. Mittemeijer and co-workers [34,35] have extensively studied in the past the kinetics of tempering reactions in Fe–C and Fe–N martensites using DTA. Besides, they [36–38] have also used DTA along with precision dilatometry to investigate certain basic issues related to the mechanism of austenite decomposition upon cooling in dilute substitutional iron-based alloys. Recently, Rajic and co-workers [32] have conducted DTA and dilatometry measurements on the tempering behaviour of quenched and hot-rolled, low-alloy, low-carbon steels. Quite similar to the findings of this study, an exothermic peak around 893 K has been observed in their DTA profile of a martensite sample. Furthermore, Nath et al. [39] have used DTA in their study of the thermal stability of austenite in a manganese-containing low-alloy, low-carbon steel. Not withstanding such extensive literature on the application of thermal analysis and related tools to study phase transformations in steels, there seems to be a paucity of information with regard to the measurement of thermodynamic properties of Cr–Mo steels, especially

Table 2 Values of coefficients in $C_P(T) = A + BT + CT^2 + DT^{-2} + E\ \exp(FT^*)(T^*)^G$ used for fitting the measured specific-heat data

Sample identification	Temp (K)	A ($J \cdot kg^{-1} \cdot K^{-1}$)	B ($J \cdot kg^{-1} \cdot K^{-2}$)	C ($J \cdot kg^{-1} \cdot K^{-3}$)	D ($J \cdot kg^{-1} \cdot K^{-1}$)	E ($J \cdot kg^{-1} \cdot K^{-1}$)	F	G
Pure iron	$T < 1{,}040$ K	2.05825×10^4	−30.44795	0.01372	-3.00273×10^9	18.76769	9.57686	−0.4796
	$T > 1{,}040$ K	2.059102×10^4	−29.92756	0.00942	-4.223212×10^9	4.88097×10^3	0.43795	−0.00978
9 Cr–1Mo N&T	$T < 1{,}013$ K	2.11379×10^4	−33.55769	0.01621	-2.585812×10^9	7.4531	10.96518	−0.38618
	$T > 1{,}013$ K	-1.638255×10^6	2.014740×10^3	−0.69629	3.211966×10^{11}	9.23525×10^2	−4.73754	0.15369
	(1,100–1,165) K	-4.673832×10^7	5.44656×10^4	−17.83752	1.0169×10^{13}	7.50856×10^3	−16.09265	0.00335
9 Cr–1Mo	$T < 1{,}014$ K	2.14514×10^4	−32.68614	0.01492	-2.972980×10^9	24.27478	9.52885	−0.19959
550 °C/500 h	$T > 1{,}014$ K	2.103423×10^4	−33.04859	0.01477	-3.000657×10^9	7.56331×10^2	−7.99835	−0.04972
aged	(1,100–1,165) K	-1.469058×10^7	1.72207×10^4	−5.67439	3.1626×10^{12}	1.3751×10^3	−59.27955	0.02756
9 Cr–1Mo	$T < 1{,}014$ K	2.051805×10^4	−31.16466	0.01403	-2.840258×10^9	20.43526	9.63457	−0.29279
550 °C/5,000 h	$T > 1{,}014$ K	2.022076×10^4	−31.35508	0.014	-3.168230×10^9	8.47936×10^2	−12.52792	−0.01597
aged	(1,100–1,165) K	-2.147145×10^7	2.49193×10^4	−8.12826	4.706×10^{12}	7.17043×10^3	−6.92634	0.00046
9 Cr–1Mo	$T < 1{,}015$ K	2.064892×10^4	−28.29548	0.01201	-3.588535×10^9	87.76339	7.90026	−0.1691
650 °C/500 h	$T > 1{,}015$ K	2.965835×10^4	−23.90832	0.00432	-9.65624×10^9	3.35509×10^2	−40.54832	−0.09203
aged	(1,100–1,165) K	-3.890724×10^7	4.55225×10^4	−14.96943	8.4061×10^{12}	-1.36454×10^5	−14.5786	1.0535
Martensite	(550–890) K	2.015337×10^4	−27.38709	0.01176	-3.9252197×10^9	2.09290×10^2	6.92206	0.08336
	(944–1,010) K	2.545662×10^4	−25.1091	0.0071	-6.554443×10^9	2.52460×10^2	−56.9628	0.05029
	$T > 1{,}010$ K	2.516467×10^4	−24.95996	0.00769	-7.690315×10^9	7.4269×10^2	−20.04515	−0.01771
	(1,100–1,165) K	-2.9055×10^7	3.3966×10^4	−11.1588	6.2806×10^{12}	4.8530×10^3	−17.18376	0.00163

under different microstructural conditions. Therefore, it is somewhat difficult to carry out a comparison of the results of this study with similar ones in the literature.

However, as can be inferred from the results of this study, thermal ageing produces small, but distinct changes in the overall heat capacity versus temperature behavior of 9Cr–1Mo steel. In general terms, the observed behavior is in-line with the expected microstructural changes that take place in these materials upon continuous ageing. Thus, taking the case of martensite for an example, the initial response is one of relaxation of a highly dislocated and hard lath martensitic microstructure resulting in the gradual development of a strain-free ferrite matrix characterized by the development of low-energy grain and sub-grain structures. This is a continuous process and is characterized by a relatively broad exothermic smearing of the DSC profile. No sharp peak as is characteristic of a precipitation reaction will be evident for initial martensite relaxation (Fig. 5). This is followed by carbide precipitation at higher temperatures. Phase stability calculations as well as experimental results on long-term aged samples in generic 9Cr–1Mo steels reveal that its is mostly the $M_{23}C_6$-type carbide that comes out under equilibrium conditions at about 650 °C upon heating and the corresponding equilibrium fraction of the carbide precipitate is rather small [18]; thus, the net C_P of a low-carbon tempered martensitic–ferritic steel is derived predominantly from the matrix ferrite phase only. Nevertheless, the presence of carbides and their morphology do play a significant role in deciding the kinetics of austenite formation and hence in determining the rate of C_P change, especially around the phase transformation region.

The carbide precipitation, being a diffusion-controlled process, is somewhat sluggish at low temperatures and requires about 650 °C to get initiated. The rate of heating plays a crucial role in the complete realization of the carbide formation and its subsequent dissolution at high temperatures, that is, upon reaching Ac_3. The slower the rate of heating, the better are the chances for the system to simulate the equilibrium transformation behavior. In this sense, the prolonged isothermal ageing at 823 K or 923 K, temperatures which are lower than Ac_1, does indeed help in establishing the equilibrium volume fraction of the minor carbide phases, with, of course, the equilibrium composition. This probably is the reason for the comparatively lower values of C_P recorded for 823 K/5,000 h aged samples, because in this case the carbide particle density should have attained the maximum possible value.

Another noteworthy outcome of this study is the estimation of the enthalpy of carbide precipitation from the martensitic microstructure. A preliminary literature search on 9Cr–1Mo steel has not yielded any precise information on this quantity. In this study, a value of about $5.6\,J \cdot g^{-1}$, which roughly translates into $302\,J \cdot mol^{-1}$ has been obtained; but as mentioned before, it is instructive to study this precipitation phenomenon at lower rates of heating to ensure the near attainment of equilibrium precipitation behavior. This point is currently under investigation. The enthalpy change associated with the $\alpha \rightarrow \gamma$ transformation in aged samples is slightly less than the corresponding value recorded for pure iron, and this is certainly due to the presence of the carbide phase that serves to retard the kinetics of the $\alpha \rightarrow \gamma$ structural change [28]. In the case of the martensite, the carbide volume fraction formed during continuous heating being relatively less, the $\alpha \rightarrow \gamma$ structure change is facilitated to a little more extent with the concomitant effect of recording a slightly higher value for enthalpy change (Table 1).

5 Conclusions

(i) The data on the temperature variation of specific heat have been generated for differently aged samples of 9Cr–1Mo steel. It is found that ageing brings about subtle modifications to the heat capacity values, especially in its temperature variation around the magnetic and α-ferrite + carbide $\rightarrow$ γ austenite phase transformation regime.

(ii) The transformation temperatures are only mildly sensitive to ageing-induced changes in the microstructure; however, the associated transformation enthalpies are more reflective of the role of the microstructure.

(iii) Prolonged ageing in the range of 823 K to 923 K (550 °C to 650 °C) results in a reduction of the heat capacity due to the presence of carbides.

(iv) The isochronal ageing of martensite is confirmed by an exothermic carbide precipitation event at 923 K (650 °C). This is attributed to the onset of $M_{23}C_6$ carbide precipitation from martensitic microstructure.

Acknowledgments The authors acknowledge Dr. K. Bhanusankara Rao, Dr. P. R. Vasudeva Rao, and Dr. Baldev Raj for their sustained support and encouragement during the course of this work. The samples used in this study are courtesy of Mr. V. Chaswal. Mr. B. Jeyaganesh wishes to acknowledge the support of DAE, for the grant of JRF fellowship at IGCAR.

References

1. T. Fujita, ISIJ Int. **32**, 175 (1992)
2. J.W. Davis, J. Nucl. Mater. **122/123**, 3 (1984)
3. R.L. Klueh, K. Ehrlich, F. Abe, J. Nucl. Mater. **191–194**, 116 (1992)
4. R.L. Klueh, *ORNL/TM-2004/176*, Nov. 2004, pp. 1–66
5. M. Tokiwai, M. Horie, K. Kako, M. Fujiwara, J. Nucl. Mater. **204**, 56 (1993)
6. S. Ukai, M. Harada, H. Okada, M. Inoue, S. Nomura, S. Shikakura, K. Asabe, T. Nishida, M. Fujiwara, J. Nucl. Mater. **204**, 65 (1993)
7. M. Tamura, H. Hayakawa, M. Tamimura, A. Hishinuma, T. Kondo, J. Nucl. Mater. **155–157**, 620 (1988)
8. J. Orr, F.R. Beckitt, G.D. Fawkes, in *Ferritic Steels for Fast Reactor Steam Generators*, ed. by S.F. Pugh, E.A. Little (BNES, London, 1978), pp. 91–109
9. S.J. Sanderson, in *Ferritic Steels for Fast Reactor Steam Generators*, ed. by S.F. Pugh, E.A. Little (BNES, London, 1978), pp. 120–127
10. A. Bjarbo, M. Hatterstrand, Mater. Trans. **32A**, 19 (2001)
11. D.V. Shtansky, G. Inden, Acta Metall. **45**, 2862 (1997)
12. M. Taneike, K. Sawada, F. Abe, Metall. Mater. Trans. A**35**, 1255 (2004)
13. N. Fujita, H.K.D.H. Bhadeshia, ISIJ Int. **41**, 626 (2001)
14. H.K.D.H. Bhadeshia, ISIJ Int. **41**, 626 (2001)
15. J.M. Vitek, R.L. Klueh, Metall. Mater. Trans. A**14**, 1047 (1983)
16. A. Kroupa, J. Havrankova, M. Coufalava, M. Svoboda, J. Vrestal, J. Phase Equilib. **22**, 312 (2001)
17. J. Hald, L. Korcakova,. ISIJ Int. **43**, 420 (2003)
18. A. Schneidner, G. Inden, Acta Mater. **53**, 519 (2005)
19. V. Vodaraek, A. Strang, Mater. Sci. Tech. **16**, 1207 (2000)
20. S. Raju, B. Jeyaganesh, A. Banerjee, E. Mohandas, Mater. Sci. Eng. **A465**, 29 (2007)
21. D.V. Shtansky, K. Nakai, Y. Ohmori, Z. Metallkd. **90**, 25 (1999)
22. S. Raju, N.S. Arun Kumar, B. Jeyaganesh, E. Mohandas, U. Kamachi Mudali, J. Alloy. Compd. **440**. 173 (2007)
23. Q. Chen, B. Sundman, J. Phase Equilib. **22**, 631 (2001)
24. P.D. Desai, J. Phys. Chem. Ref. Data **15**, 967 (1986)

25. T.M.V.R. de Barros, R.C. Santos, A.C. Fernandes, M.E. Minas da Piedabe, Thermochim. Acta **269/270**, 51 (1995)
26. M.J. Richardson, in *Compendium of Thermophysical Property Measurement Techniques,* vol. 2, ed. by K.D. Maglic, A. Cezairliyan, V.E. Peletsky (Plenum Press, New York, 1992), p. 519
27. B. Nath, E. Metcalfe, J. Hald, in *Microstructural Development and Stability in high Chromium Ferritic Steels*, ed. by A. Strang, D.J. Gooch (The Institute of Materials, London, 1997), p. 123
28. U.R. Lenel, Scripta Metall. **47**, 471 (1983)
29. U.R. Lenel, R.W.K. Honeycombe, Met. Sci. **18**, 201 (1984)
30. C.G. de Andres, F.G. Caballero, C. Capdevila, L.F. Alvarez, Mater. Charact. **48,** 101 (2002)
31. A.T.W. Kempen, F. Sommer, E.J. Mittemeijer, Thermochim. Acta **383**, 21 (2002)
32. M. Gojic, M. Suceska, M. Rajic, J. Therm. Anal. Calorim. **75**, 947 (2004)
33. G.P. Krielaart, C.M. Brakman, S. Van der Zwaag, J. Mater. Sci. **31**, 1501 (1996)
34. M. Van Rooyen, E.J. Mittemeijer, Scripta Metall. **16**, 1255 (1982)
35. P.V. Morra, A.J. Bottger, E.J. Mittemeijer, J. Therm. Anal. Calorim. **64**, 905 (2001)
36. A.T.W. Kempen, F. Sommer, E.J. Mittemeijer, Acta Mater. **50**, 3545 (2002)
37. F.C. Liu, F. Sommer, E.J. Mittemeijer, Acta Mater. **51**, 507 (2003)
38. F.C. Liu, F. Sommer, E.J. Mittemeijer, Acta Mater. **52**, 2549 (2004)
39. S.K. Nath, S. Ray, V.N.S. Mathur, M.L. Kapoor, ISIJ Int. **34**, 191 (1994)